Modeling Electronic Properties of Correlated Materials Using First Principles

Saisrinivas Gudivada[1] and Betül Pamuk[2]
[1] *Department of Physics, University of California, Berkeley, Berkeley, CA 94720, USA*
[2] *Department of Physics, Cornell University, Ithaca, New York 14853, USA*

(Dated: August 22, 2022)

We analyzed the electronic structure of four strongly correlated materials - $SrVO_3$, $NbSe_2$, $KTaO_3$, and $KNbO_3$. The data for $SrVO_3$ and $NbSe_2$ was sent to our collaborators Dr. Brendan Faeth and his mentee Anna Capuano, who compared our calculations with their Angle-Resolved Photoemission Spectroscopy (ARPES) measurements. Our calculation of the Γ point conduction band of $SrVO_3$ was a near exact match compared to the experimental Fermi surface. We studied the effect of strain on the electronic structure $KTaO_3$, which we found to have an overall marginal impact relative to bulk $KTaO_3$, and explored the electronic structure of $KNbO_3$.

I. Introduction

Strongly correlated materials possess numerous qualities that make them appealing in industry and academia.[1,2,3,4] $SrVO_3$ (cubic lattice) is optically transparent, conductive, and has tunable electron mobility. $NbSe_2$ (hexagonal lattice) is ferromagnetic, has a Charge Density Wave, and can be superconductive. $KTaO_3$ (cubic lattice) is optically transparent, shows spin transport, and can also be superconductive, while $KNbO_3$ (cubic lattice, but has different phase geometries) is optically transparent, piezoelectric, and exhibits phase-based polarity.

These four materials were the crux of our research, which consisted of two goals. First, to conduct theoretical calculations on the electronic properties of $SrVO_3$ and $NbSe_2$ and collaborate with the PARADIM ARPES team, who would compare our results with their experimental measurements of the Fermi surface of the materials. They would then integrate the data we provided into proprietary software that directly compares our data with real-time measurements of the material's Fermi surface. Second, to investigate if a non-polar material like $KTaO_3$ could become ferroelectric when strain is applied and compare with polar phases of $KNbO_3$ to examine conditions for the formation of polarity.

II. Methodology

Density Function Theory (DFT) is described by the Kohn-Sham Equations, which are used to calculate the energies of a system:

$$[T + v_{ext}(r) + v_H(r) + v_{xc}(r)]\phi_i(r) = E_i\phi_i(r).$$

, where $\phi_i(r)$ is the i'th electron wave function, T is the kinetic energy of the electrons, $v_{ext}(r)$ is the Coulomb attraction between the nucleus and the electrons, $v_H(r)$ is the Hartree potential (Coulomb repulsion between electrons), and v_{xc} is the Exchange-Correlation (XC) energy. However, DFT does not know the exact form of the XC energy in the system. Thus, functionals (functions that take other functions and output a scalar value) are used to determine the XC energy by taking input parameters such as the electron density of the system - $n(r) = \sum_i |\phi_i(r)|^2$ - and its Taylor expansions.

All electronic structures were computationally calculated using DFT through the Quantum Espresso software[6] on the Rockfish cluster courtesy of Johns Hopkins University: from which energies, band structures, and Density of States (DOS) were obtained. $SrVO_3$ was calculated using the PBE functional, a 24x24x24 k-mesh, an energy cutoff of 80 Ry, and cold smearing of 0.005 Ry. $NbSe_2$ was calculated using the PBE functional, a 24x24x6 k-mesh, an energy cutoff of 170 Ry, and cold smearing of 0.005 Ry. $KTaO_3$ was calculated using the PBE functional, a 24x24x24 k-mesh, and an energy cutoff of 150 Ry. $KNbO_3$ was calculated using the PBE functional, a 24x24x24 k-mesh, and an energy cutoff of 150 Ry. Note that $KTaO_3$ and $KNbO_3$ have no smearing as they are not metals.

III. Results

We compared the structure calculations for each metal with attributes based on previous literature to determine the validity of our results. Note that the calculations for NbSe2 are based on the initial atomic positions of the atom and have not been relaxed and that the Brillouin zones pictured are courtesy of SeeK-path[5].

A. Goal I

1. $SrVO_3$

$SrVO_3$ is a metal - which means that the Fermi level passes through the conduction band - and has the following properties: a bandwidth of between 0.9 and 2.6 eV at the conduction band, while the Γ point of the conduction band is between -1 and -0.4 eV.[1] Based on Figure 1, the bandwidth of the conduction band is about 2 eV, and the Γ point of the conduction band is around -1 eV. Thus, our results for $SrVO_3$ corroborate with past literature.

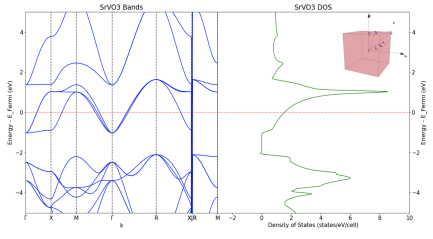

Figure 1: Band Structure and DOS of $SrVO_3$.

Additionally, our collaborators found a near exact match in the gamma point conduction band between our calculations and their measurements of $SrVO_3$'s Fermi surface, as shown in Figure 2.

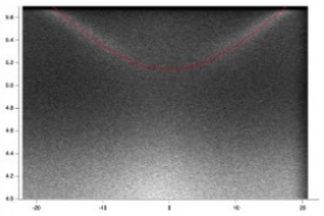

Figure 2: Measurement of Fermi surface of $SrVO_3$, with DFT calculation denoted by the red line.

2. $NbSe_2$

$NbSe_2$ is a metal and has the property that after crossing the Fermi level, the gap between the conduction and valence band is from 0.35 to 0.6 eV.[2] Based on Figure 3, the area between the two purple lines has a height that varies from about 0.35 to 0.6 eV. Figure 3 also details the calculation of $NbSe_2$ using spin-orbit coupling (SOC), which includes relativistic effects for electron interactions. The main difference between the relativistic and scalar calculations is the increased number of avoided crossings in the relativistic calculation due to more electron interactions in the system.

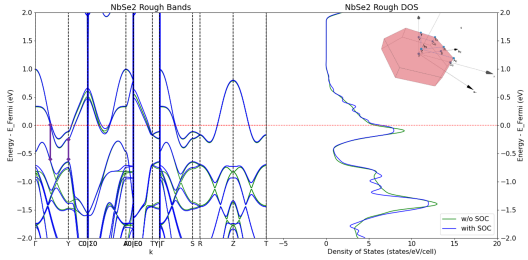

Figure 3: Band Structure and DOS of $NbSe_2$.

B. Goal II

1. $KTaO_3$

$KTaO_3$ is an insulator, which means that there is a gap between the conduction and valence bands larger than 2 eV and that the Fermi level lies directly on the maxima of the valence band.[3] Based on the left panel of Figure 4, $KTaO_3$ has a band gap wider than 2 eV.

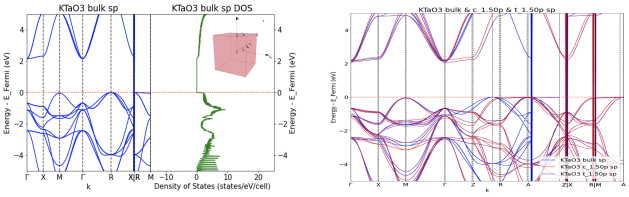

Figure 4 (left): Band Structure and DOS of $KTaO_3$. (right): Band Structure of bulk, 1.5 percent compressive strain, and 1.5 percent tensile strain $KTaO_3$.

Strain calculations of $KTaO3_3$ were also conducted between ± 3 percent, with ± 0.55 and 1.5 percent being the primary focus. The right panel of Figure 4 shows the variation between the bulk and respective compressive and tensile strains of 1.5 percent. Note that the strained structures have a different and longer k-path, as the geometry has changed from cubic to tetragonal, and that - in relation to bulk - the tensile strain has a lower band gap, while the compressive strain has a slightly higher band gap.

2. $KNbO_3$

Cubic $KNbO_3$ is a semi-conductor, which means that there is a gap between the conduction and valence bands that is less than 2 eV and that the Fermi level lies directly on the maxima of the valence band.[4] Based on Figure 5, $KNbO_3$ has a band gap smaller than 2 eV.

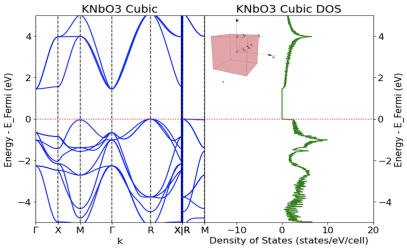

Figure 5: Band Structure and DOS of $KNbO_3$.

IV. Future Work

In the future, we can optimize the structure of $NbSe_2$, do calculations of the bands and DOS for different $KNbO_3$ phases (especially polar phases), and phonon measurements on different $KTaO_3$ strains to determine instabilities that might lead to polarity in the material.

Acknowledgments

I would like to thank PARADIM and Cornell for hosting me this summer, Johns Hopkins for providing the Rockfish cluster, My mentor Dr. Betül Pamuk for her expert guidance and keen insight, Professor Darrell Schlom for being my PI, Dr. Brendan Faeth for being a wonderful collaborator, and Jim Overhiser for being an excellent coordinator. This work is supported by the National Science Foundation (Platform for the Accelerated Realization, Analysis, and Discovery of Interface Materials (PARADIM)) under Cooperative Agreement No. DMR-2039380 and National Science Foundation (REU Site: Summer Research Program at PARADIM) under Cooperative Agreement No. DMR-2150446.

References

[1] R. Sakuma, Ph. Werner, and F. Aryasetiawan, Phys. Rev. B 88, 235110 (2013).

[2] José Ángel Silva-Guillén et al 2016 2D Mater. 3 035028.

[3] Bouafia, H., Hiadsi, S., Abidri, B., Akriche, A., Ghalouci, L., & Sahli, B. (2013). Structural, elastic, electronic and thermodynamic properties of KTaO3 and NaTaO3: AB initio investigations. Computational Materials Science, 75, 1-8. https://doi.org/10.1016/j.commatsci.2013.03.030.

[4] Wang, D., Wang, G., Lu, Z., Al-Jlaihawi, Z., & Feteira, A. (2020). Crystal structure, phase transitions and Photoferroelectric properties of knbo3-based lead-free ferroelectric ceramics: A brief review. Frontiers in Materials, 7. https://doi.org/10.3389/fmats.2020.00091.

[5] Materials Cloud. (n.d.). SeeK-path. https://www.materialscloud.org/work/tools/seekpath.

[6] Quantum Espresso. (2022, March 22). https://www.quantum-espresso.org/.